RJC

RASĀYAN *J. Chem.*
Vol. 18 | No. 1 |325-333| January - March | 2025
ISSN: 0974-1496 | e-ISSN: 0976-0083 | CODEN: RJCABP
http://www.rasayanjournal.com
http://www.rasayanjournal.co.in

In vitro ANTIBACTERIAL AND *in vivo* WOUND HEALING PROPERTIES OF BIOSYNTHESIZED ZnO NANOPARTICLES WITH *Dalbergia sissoo* EXTRACT

Ashwini Singhal[1], Gyan Prakash Meghwal[2], Anita Kumari[1], Nighat Fahmi[1], R.V. Singh[1], Priyadharshi Meena[2] and Ramhari Meena[1,✉]

[1]Department of Chemistry, University of Rajasthan, Jaipur-302004, (Rajasthan) India
[2]Department of Zoology, University of Rajasthan, Jaipur-302004, (Rajasthan) India
✉Corresponding author: ramharichem@gmail.com

ABSTRACT

In this study, we enforced a sustainable and efficient approach to synthesizing zinc oxide nanoparticles (ZnO-NPs) by employing the *Dalbergia sissoo* leaf extract. Biosynthesized ZnO-NPs have been characterized by various techniques (XRD, TEM, FT-IR, UV-VIS, FESEM and EDX). The ZnO-NPs exhibited a prominent absorption peak at 288 nm in the UV-Vis spectrum, indicating their optical characteristics. X-ray diffraction (XRD) pattern confirmed that these nanoparticles were crystalline, specifically displaying a hexagonal wurtzite phase. The FESM images showed a range of surface morphologies for the ZnO-NPs, from irregular shapes to nearly spherical forms. XRD and TEM analysis obtained that the ZnO-NPs have average crystallite sizes of 15.86 nm and 18.68 nm, respectively. ZnO-NPs demonstrated antimicrobial effectiveness against gram-positive (*S. aureus, B. subtilis*) and gram-negative (*E. coli, P. aeruginosa*) bacteria strains. B. subtilis exhibited the most significant inhibition zone, measuring 22.5 ± 0.18 mm at a 100 µg/mL concentration. In vivo studies conducted with mice have demonstrated that synthesized ZnO-NPs exhibit significant potential for promoting wound healing. These investigations reveal that applying ZnO-NPs leads to enhanced tissue regeneration and accelerated healing processes, suggesting their promising role in wound treatments.

Keywords: Biosynthesis, *Dalbergia sissoo*, ZnO-NPs, Antibacterial activity,Wound healing potency
RASĀYAN*J. Chem.*, Vol. 18, No.1, 2025

INTRODUCTION

Nanotechnology, expressed as the precise manipulation of materials at the atomic or molecular scale with at least one dimension measuring in nanometers, has rapidly emerged as a transformative interdisciplinary research field.[1] This innovative field offers significant potential due to its expansive range of advanced applications, influencing nearly every facet of contemporary life in fields such as medicine[2], electronics[3], environmental science[4], and energy solutions[5]. Metal and metal oxide nanoparticles are increasingly important due to their wide-ranging applications.[6] Nanomaterials enhance catalysis, improve electronics, and optimize light manipulation.[7] They boost energy storage and conversion performance, aid in environmental remediation, and hold potential in biomedicine for drug delivery and imaging. Additionally, they are used in sensing devices for environmental and health monitoring.[8] The current literature thoroughly summarizes the different methods used in synthesizing nanomaterials, which can be broadly grouped into three main categories: physical, chemical, and electrochemical approaches.[9] The traditional methods of synthesizing nanoparticles often involve chemical processes that carry risks like contamination and toxicity. As a result, there has been a growing interest in alternative approaches, mainly green chemistry, which utilizes biological resources such as plants and microorganisms. Among these, plant extracts are highly effective for nanoparticle synthesis.[10] Advancing environmentally friendly processes that leverage natural products is essential for the progress of nanotechnology.[11] ZnO-NPs have garnered substantial interest in various fields because of their remarkable properties and vast potential applications.

Traditional methods for synthesizing ZnO-NPs lead to hazardous by-products that pose risks to human health and the environment. Green chemistry offers innovative and cost-effective methods for producing ZnO-NPs by harnessing naturally occurring resources.[12] One promising strategy is plant-mediated

http://doi.org/10.31788/RJC.2025.1819211

synthesis, which utilizes various plant components such as leaves, stems, roots, and flowers to convert metal ions into nanoparticles. This biological method reduces the creation of harmful substances and improves the synthesis process's overall efficiency.[13] In summary, these sustainable techniques contribute to a more eco-friendly approach to nanotechnology, fostering advancements across various applications while promoting responsible and sustainable practices in chemistry. Plant-derived ZnO-NPs are versatile materials with many applications across multiple fields.[14] They are utilized in biomedicine, drug delivery, and cancer treatment, as well as in water purification, the cosmetics industry, electronics, and sensor technology.[15] The current study focused on synthesizing and characterizing ZnO-NPs derived from the leaf extract of *Dalbergia sissoo*. Various techniques were utilized to comprehensively characterize these biosynthesized ZnO-NPs and explore their potential biological activities, including *in vitro* antibacterial properties and *in vivo* wound healing efficacy.

EXPERIMENTAL

Chemicals, Reagents and Plant Source

Sigma-Aldrich provided the zinc(II) acetate dihydrate ($Zn(CH_3CO_2)_2 \cdot 2H_2O$). At the same time, the leaves of *Dalbergia sissoo* were sourced directly from the Department of Botany at the University of Rajasthan in Jaipur, Rajasthan, India. Before their use in the synthesis procedure, all glassware is thoroughly cleaned using aqua regia and subsequently rinsed with double-distilled water.

Preparation of leaf extract

D. sissoo leaves were collected, cleaned, and dried for two weeks after contaminants were removed. They were then dried in a hot-air oven at 50°C for five hours, chopped into small pieces, and ground into a powder using a mortar and pestle. Preparing the plant leaf extracts involved combining 20 grams of powdered leaves with 100 mL of distilled water in a beaker. This mixture was gently heated to 70°C for 90 minutes while stirring consistently. Behind the heating process, the mixture was filtered using Whatman No. 1 filter paper and allowed to cool. The resulting *D. sissoo* extract was then stored in the refrigerator at 4°C (Fig.-1).

Preparation of ZnO-NPs

In the green synthesis method (Fig. 1), 20 mL of *D. sissoo* extract was combined with 80 mL of 0.01 M zinc(II) acetate dihydrate solution in a 250 mL Erlenmeyer flask. The mixture was brought to a temperature of 50°C and stirred for 2 hours. During this process, the solution gradually changed to brown due to adding *D. sissoo* leaf extract. Afterwards, the mixture was left to sit at room temperature for 24 hours. It was centrifuged at 12,000 rpm for 15 minutes to separate the components effectively. The nanoparticles were produced by evaporating the separated solution in a hot oven set to 400°C for three hours (Fig.-1).

Characterization of synthesized nanoparticles

Fourier-transform infrared (FT-IR) spectra for the samples were captured using a Perkin Elmer model (Spectrum Two) within a frequency span of 400–4000 cm^{-1}. The optical characteristics of ZnO-NPs were investigated by thoroughly analyzing the peaks obtained from a UV-visible spectrophotometer (Agilent Technologies Cary 60). The dimensions of the nanoparticles were evaluated through transmission electron microscopy (Tecnai G2 S-TWIN, 200 kV). The UV-Vis spectrum was measured across a wavelength interval ranging from 200 to 800 nm. The X-ray diffraction (XRD) pattern for the ZnO-NPs was acquired using the XPERT PRO PANAlytical XRD system. Furthermore, the morphology and elemental mapping of the ZnO-NPs were investigated using field emission scanning electron microscopy (Apreo 2S Highvac, Thermo Fisher Scientific) equipped with energy-dispersive X-ray spectroscopy (EDX).

In vitro antibacterial activity of ZnO-NPs

The antibacterial properties of ZnO-NPs were evaluated *in vitro* against gram-positive bacteria, specifically *B. subtilis* and *S. aureus*, and gram-negative bacteria, namely *P. aeruginosa* and *E. coli*, utilizing the Agar Well Diffusion method. Four concentrations of ZnO-NPs were prepared (25µg/mL, 50

µg/mL, 75 µg/mL, and 100 µg/mL) in a solution containing 0.5% dimethyl sulfoxide (DMSO). Nutrient agar plates were inoculated with specific bacterial strains and prepared with wells for testing. ZnO-NPs and Streptomycin (30 µg/mL) were added to these wells. After 24-hour incubation at 37 ºC, inhibition zones were measured to assess antibacterial activity, and the mean values and standard deviations were calculated from triplicate experiments.

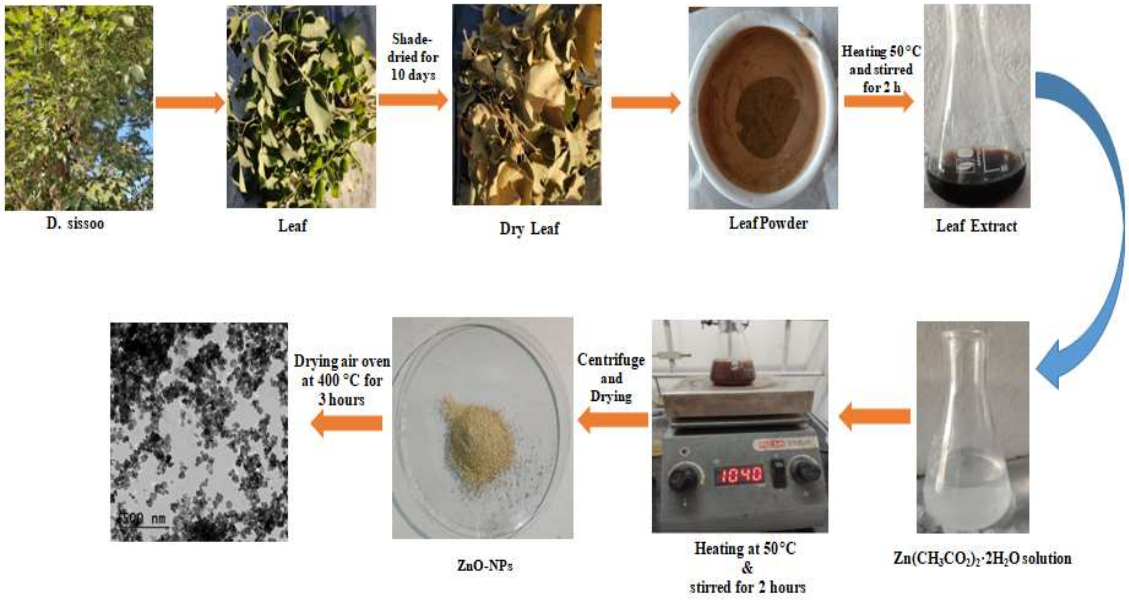

Fig.-1: Schematic diagram of the green synthesis of ZnO-NPs using an aqueous extract of *D. sissoo.*

In vivo wound healing activity of ZnO-NPs

Preparation of Vaseline ointment containing ZnO-NPs

To prepare Vaseline ointment with ZnO-NPs, heat 30 grams of pure Vaseline in a water bath at 60 °C using the bain-marie technique to prevent degradation. Once melted, add 0.3 grams of ZnO-NPs (1% w/w) and mix thoroughly for uniform distribution. Then, sonicate the mixture at 60 °C for 30 minutes to break down agglomerations and enhance dispersion, resulting in a consistent, smooth ointment.

Animal care and handling

The present study involved male Swiss albino mice weighing 25 to 30 grams. The animals were obtained from the Central Animal Facility (CAF) at the National Institute of Pharmaceutical Education and Research (NIPER), Mohali, Chandigarh (Reg. No: (108/GO/Re/Rc/Bi/Bt/99/CPCSEA). All animal experiment procedures were carried out by the standards set forth by the Institutional Animal Ethical Committee at the Department of Zoology, University of Rajasthan, located in Jaipur, India. The committee provided its official approval, documented in letter number UDZ/IAEC/V/07, dated March 16, 2022, ensuring that our research adheres to ethical guidelines and prioritizes the animals' welfare. The experimental work involved animals housed at the Department of Zoology, University of Rajasthan, Jaipur, under controlled conditions (temperature: 20–30°C, humidity: 50–70%, 12:12 light: dark cycle). After a 7-day acclimatization period, the study assessed the wound healing potential of biosynthesized ZnO-NPs in three groups:

Group A: Control Group – No treatment received.
Group B: Positive Control Group – Treated with Nitrofurazone (0.2% w/w) ointment.
Group C: Drug Treated Group – Treated with vaseline ointment containing ZnO-NPs.
Animals had ad libitum access to dry pellets and tap water.

Excision wound model

Excisional wounds serve as a valuable model for studying wound healing, particularly acute clinical wounds requiring healing without sutures. In this study, animals were anesthetized with diethyl ether, and

their dorsal backs were shaved to prepare for the wound creation. The shaved area was treated with 70% ethanol to ensure antiseptic conditions. A circular excisional wound was then made, extending through the entire thickness of the skin in the designated area, and no dressing was applied afterward. Importantly, no antimicrobial agents were administered locally or systemically. Each mouse was housed individually throughout the experiment to evaluate the healing efficacy of ZnO-NPs while eliminating the effects of antimicrobial treatments. Additionally, the study used nitrofurazone ointment at a concentration of 0.2% w/w as a positive control. This approach allowed for a comprehensive assessment of natural wound recovery with and without the application of the drug treatment.

Determination of wound contraction

After creating the excisional wounds, the experimental animals were divided into three distinct groups, as previously outlined in our study. To ensure precise evaluation, the margins of these excision wounds were carefully marked with a transparent plastic sheet, facilitating accurate measurement. The area of each wound was assessed using a method known as planimetry, which involved placing the transparent sheet over graph paper to quantify the size of the wounds in square millimeters. This meticulous process was repeated daily throughout the observation period to monitor changes. Additionally, high-resolution images of the dorsal surfaces of the mice were taken on the 1st, 6th, 12th, and 18th days of the healing process, providing a visual record of the progression. To evaluate the effectiveness of wound healing, the percentage of wound contraction was calculated using a formula (1), which allowed for a clearer understanding of the dynamics involved in the healing process.

$$\textbf{Percent wound contraction} = \frac{\textbf{Initial wound area - unhealed area}}{\textbf{Initial wound area}} \times 100 \quad (1)$$

Statistical analysis

The results are presented as mean ± S.D. The experiment was carried out in three replicates for each treatment. The obtained data were analyzed by using one-way ANOVA and Student's t-test. Values of $p < 0.05$ indicated statistical significance.

RESULTS AND DISCUSSION

UV−vis analysis of **ZnO-NPs**

The ultraviolet-visible (UV-Vis) spectra of the biosynthesized ZnO-NPs, as shown in Fig.-2a, reveal a distinct peak at 288 nm. The distinct absorption band observed strongly suggests the successful synthesis of ZnO-NPs, underscoring their exceptional optical properties.

X-ray Diffraction (XRD) analysis of ZnO-NPs

The crystal structure of ZnO-NPs can be thoroughly examined through X-ray diffraction (XRD). As depicted in Fig.-2b, the XRD spectra of the ZnO-NPs powder reveal a distinctive hexagonal phase/Wurtzite crystal structure characterized by sharp and well-defined peaks at specific diffraction angles. These peaks, which appear prominently at angles of 32.10°, 34.68°, 36.48°, 47.83°, 56.90°, 63.02°, 66.92°, 68.28°, 69.45°, 72.87°, and 79.79°, coordinate to the Miller indices (100), (002), (101), (102), (110), (103), (200), (112), (201), (004), and (202), respectively. The findings indicate that the ZnO-NPs exhibit a hexagonal or wurtzite crystal structure, according to the JCPDS card number (00-036-1451) data. Additionally, these nanoparticles' mean crystallite size (D) was determined using the Debye–Scherrer equation (2).

$$D = \frac{\lambda k}{\beta \cos\theta} \quad (2)$$

The Debye–Scherrer equation plays a crucial role in crystallography by providing a method to estimate the size of crystalline materials. In this equation, several key variables are involved: D denotes the crystal size, k is a constant set to unity, λ represents the X-ray wavelength (precisely 1.5406 nm), β indicates the full width at half maximum (FWHM) of the diffraction peak, and θ is the diffraction angle. By applying this equation, researchers have determined that the size of ZnO-NPs is approximately 15.86 nm.

FT-IR analysis of ZnO-NPs

The ZnO-NPs synthesized using leaf extract from D. sissoo displayed distinct absorption peaks at approximately 599 cm^{-1}, 1636 cm^{-1}, 2119 cm^{-1}, and 3310 cm^{-1} (Fig.-2c). These peaks correspond to specific functional groups: the peak at 1636 cm^{-1} indicates the amide C=O stretching vibrations, while the peak at 2119 cm^{-1} reflects the stretching of the carbon-carbon triple bond (C≡C). A peak at 3310 cm^{-1} indicates the presence of amine (N-H) and hydroxyl (O-H) groups, while a peak at 599 cm^{-1} corresponds to the Zn-O bond in pure zinc oxide nanoparticles.

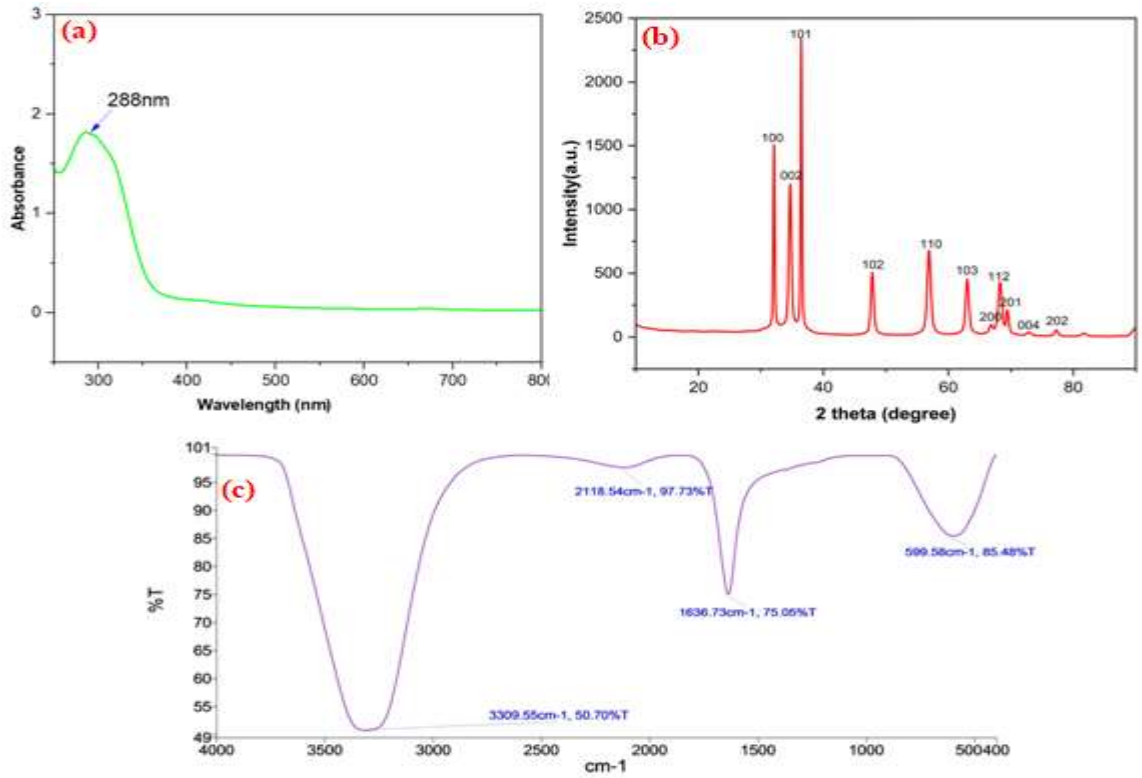

Fig-2: (a) UV Visible spectrum of ZnO-NPs. (b) Powder XRD pattern of ZnO-NPs. (c) FT-IR spectra of ZnO-NPs

FESEM, EDX and TEM analysis of ZnO-NPs

The surface morphology of ZnO-NPs is examined by field emission scanning electron microscopy (FESEM). The FESEM image reveals the uniform distribution of nearly spherical ZnO-NPs indicated in Fig.-3a. Furthermore, Fig.-3b illustrates the EDX (energy-dispersive X-ray) analysis, which successfully identifies distinct elemental signals corresponding to zinc (Zn), carbon (C), and oxygen (O) within the ZnO-NPs. The detection of elemental carbon in the EDX results is direct evidence of the biosynthesis process, highlighting the plant leaf extract's contribution in forming these nanoparticles.Transmission electron microscopy (TEM) was employed to thoroughly examine the morphology and particle size characteristics of ZnO-NPs. The observations obtained from the TEM imaging are illustrated in Fig.-3c. The detailed analysis of the TEM images indicated that the ZnO-NPs predominantly exhibit a nearly spherical shape. We used ImageJ software to conduct a detailed analysis and quantify the particle sizes. This analysis's results confirmed the ZnO-NPs sizes with a calculated average particle size of 18.68 nm, as represented in Fig.-3d.

Antibacterial assay

In this investigation, we studied the antibacterial effects of biosynthesized ZnO-NPs against two bacterial strains: gram-positive and gram-negative. The findings in Fig.-4a demonstrate that ZnO-NPs exhibit significantly stronger antibacterial effects against gram-positive bacteria. The antibacterial effectiveness of these ZnO-NPs was evaluated against four distinct pathogenic bacterial strains, as outlined in Table 1.

Streptomycin was used as a positive control to provide a benchmark for assessing the ZnO-NPs' ability to inhibit bacterial growth. This is reflected in the enhanced zones of inhibition, as depicted in Fig.-4b. The most notable antibacterial activity was recorded, with inhibition zones measuring 22.18 ± 0.55 mm for *B. subtilis* and 12.06 ± 0.43 mm for *S. aureus*, both at a concentration of 100 µg/mL. These results strongly suggest that ZnO-NPs possess a potent antibacterial effect, likely due to their ability to target and inhibit various bacterial strains. Furthermore, the surface of ZnO-NPs is enriched with various phytochemicals derived from plant extracts. These phytochemicals interact directly with the proteins in bacterial cell walls, leading to structural damage and cell rupture, which inhibits bacterial growth.

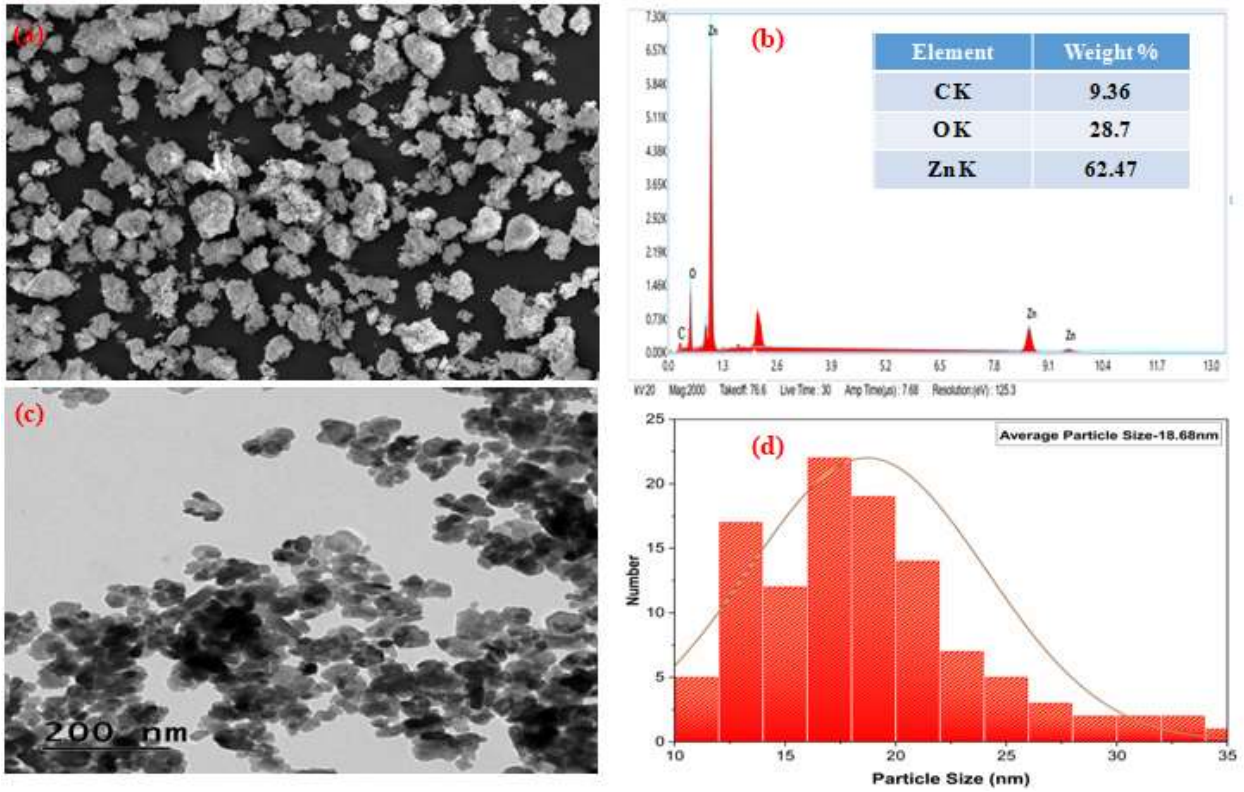

Fig.-3: (a) FESEM image of ZnO-NPs, (b) EDX analysis of ZnO-NPs, (c) TEM image of ZnO-NPs at 200 nm. (d) Particle size distribution curve.

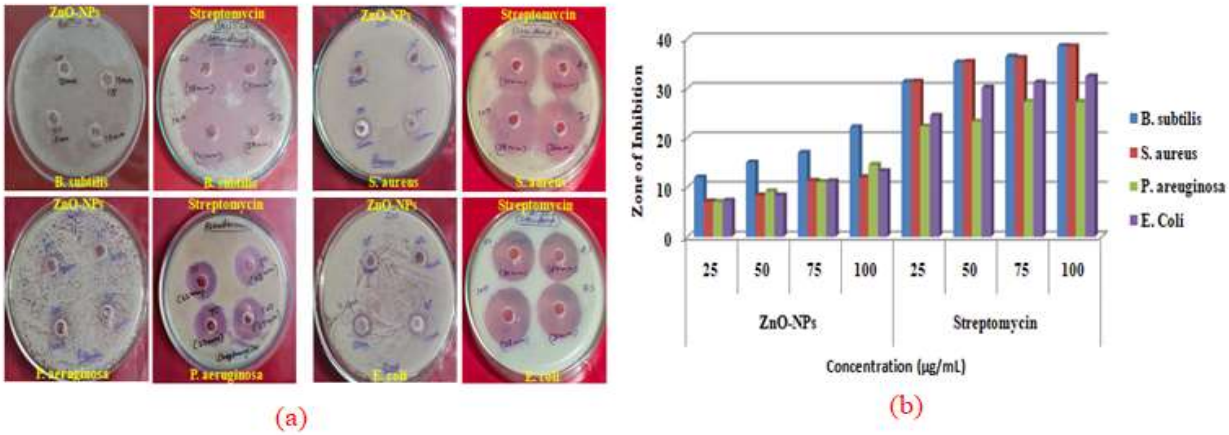

Fig.-4: (a) Zones of inhibition created by of ZnO-NPs against the bacterial strains: Gram-positive (*B. subtilis* and *S. aureus*), gram-negative (*P. aeruginosa* and *E. coli*) and and streptomycin. (b) Graphical representation of antimicrobial activity of ZnO-NPs and streptomycin on selected bacterial strains. Results are shown as means ± S.D for triplicate with error bars indicating statistical significance at $p < 0.05$.

Wound healing efficacy

A study using the excision wound model in mice evaluated the effects of ZnO-NPs on wound healing over 18 days. The treatment group showed a significant improvement, with 66.40% of wounds healed by day 10, compared to 55.56% in the negative control group. The positive control group, treated with nitrofurazone ointment, had the best outcome, healing 80.77% of wounds. Complete healing with ZnO-NPs was achieved in 16 days, while the negative control reached full recovery by day 18, and the positive control by day 14.

Table -1: Antibacterial Activity of ZnO NPs and Zone of Inhibition in mm.

Diameter of inhibition zone(mm)	Concentration in µg/mL							
	ZnO-NPs				Streptomycin			
	25	50	75	100	25	50	75	100
B. subtilis	12.03±0.61	15.20± 0.39	17.00 ± 0.54	22.18 ± 0.55	31.36± 0.44	35.12 ± 0.29	38.40 ± 0.51	41.53 ± 0.68
S. aureus	7.18 ± 0.41	8.34 ± 0.50	11.32 ± 0.38	12.06 ± 0.43	31.29± 0.28	35.27 ± 0.38	36.43 ± 0.50	38.55 ± 0.47
P. areuginosa	7.06 ± 0.47	9.18 ± 0.61	11.09 ± 0.59	14.59 ± 0.52	22.34± 0.40	23.32 ± 0.34	27.33 ± 0.43	27.30 ± 0.31
E. Coli	7.34 ± 0.31	8.39 ± 0.46	11.26 ± 0.37	13.28 ± 0.25	24.50± 0.44	30.20 ± 0.17	31.25 ± 0.29	32.45 ± 0.40

The study included visual documentation and quantitative assessments of wound contraction, revealing the effectiveness of ZnO-NPs in promoting faster wound healing. Visual documentation, including photographs taken on days 1, 6, 12, and 18, supports these impressive findings and illustrates the progressive healing phase (Fig.-5a). In addition, the study included quantitative assessments of wound contraction, carefully recorded in square millimeters, along with a thorough comparative analysis of the percentage of healed wounds across the ZnO-NPs group, the positive control cohort, and the negative control group. These findings are effectively displayed in Fig.-5b and Fig.-5c, providing valuable insights into the differing effects of the treatments on wound healing dynamics.

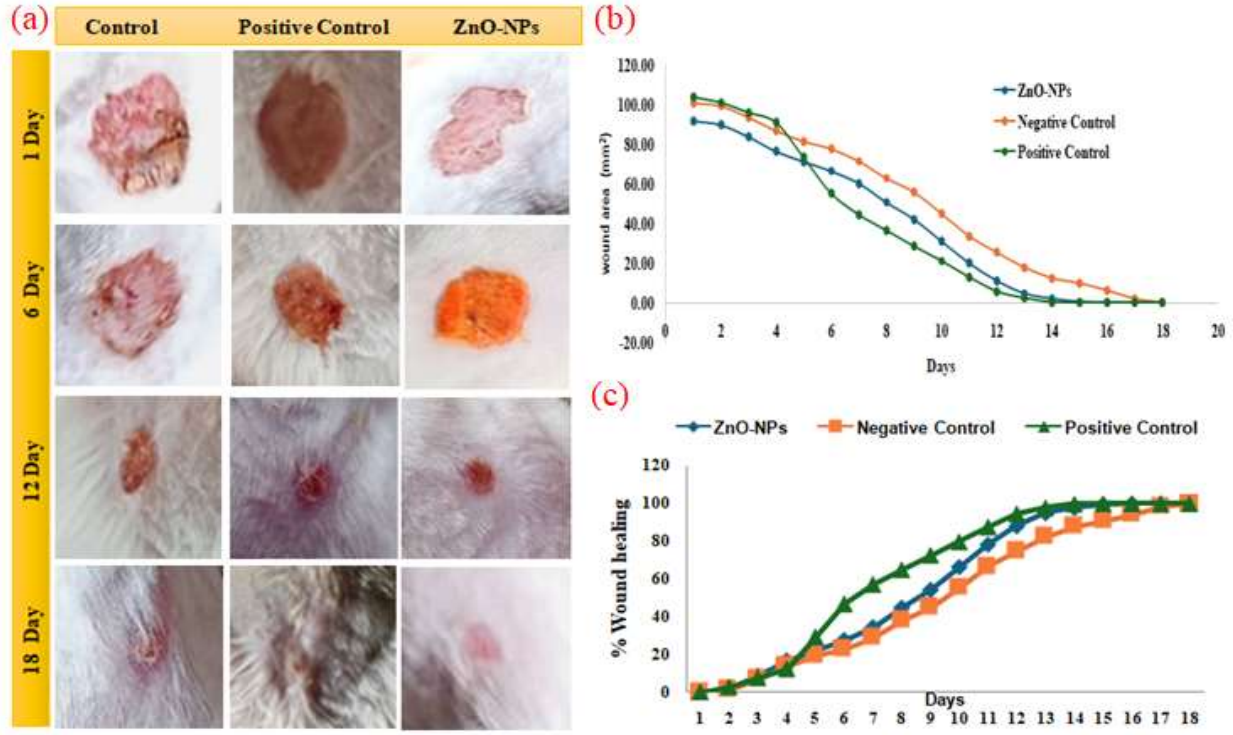

Fig.-5:*In vivo* wound healing efficacy study in mice. (a) Representative photographs during the topical treatment following the group's wound healing process. (b) Effect of treatments on wound contraction (mm^2) in wound healing. (c) A comparison of the Percentage of wounds healed between the ZnO-NPs, positive control compared to control. $P < 0.05$ statistically significant difference in comparison with the untreated group.

CONCLUSION

ZnO-NPs were successfully synthesized utilizing leaf extract from *Dalbergia sissoo*, a method characterized by being environmentally friendly and cost-effective. Various advanced techniques were

used to analyze the properties of the ZnO-NPs. FT-IR suggests that phytochemicals play a crucial role in efficiently synthesizing ZnO-NPs. The structural and morphological analyses revealed that the particle size of synthesized ZnO-NPs varied significantly, falling within a range of 10 to 35 nm. ZnO-NPs displayed a hexagonal wurtzite crystalline structure. ZnO-NPs showed significant antibacterial activity at 25, 50, 75, and 100 µg/mL concentrations. The study indicated that ZnO NPs were effective against four bacterial strains, as evidenced by observable inhibition zones. Furthermore, ZnO-NPs demonstrated effective wound-healing properties. The results were promising, indicating that wounds treated with the ZnO-NPs ointment exhibited significantly accelerated contraction rates compared to a control group, underscoring the practical applicability of these nanoparticles in therapeutic settings. Overall, this extensive research provides crucial insights into nanobiotechnology and nanomedicine, establishing a solid foundation for future studies and applications of copper oxide nanoparticles. The innovative synthesis method and the resulting nanoparticle properties present an exciting opportunity for advancing therapeutic practices in medicine and regenerative health.

ACKNOWLEDGMENTS

We would like to extend our thanks to the CSIR-University Grant Commission for providing financial assistance to one of our authors, Ashwini Singhal (Grant No. 274/(CSIR-UGC NET 2018), New Delhi, India). We thank Dr. Chitra Jain, Biomitra Life Sciences Pvt. Ltd, for their generous help during *in vitro* antibacterial experiments.

CONFLICT OF INTERESTS

The authors declare that there is no conflict of interest.

AUTHOR CONTRIBUTIONS

All the authors contributed significantly to this manuscript, participated in reviewing/editing and approved the final draft for publication. The research profile of the authors can be verified from their ORCID ids, given below:

Ashwini Singhal http://orchid.org/0000-0001-5489-5901
Gyan Prakash Meghwal https://orcid.org/ 0009-0004-5522-0147
Anita Kumari https://orcid.org/ 0000-0001-9033-1580
Nighat Fahmi https://orcid.org/0000-0002-3047-1343
R.V. Singh https://orcid.org/0000-0002-5621-4468
Priyadharshi Meena https://orcid.org/0009-0007-9731-3271
Ramhari Meena https://orcid.org/0000-0001-9073-9340

REFERENCES

1. V. Tavallali, H. Tavallali, A. Mazraeh and M. D. Darvishzadeh, *Current Research in Green and Sustainable Chemistry*, **9**, 100437(2024), https://doi.org/10.1016/j.crgsc.2024.100437
2. J.O. Gidiagba, C. Daraojimba, K.A. Ofonagoro, N.L. Eyo-Udo, B.A. Egbokhaebho, O.A. Ogunjobi and A.A. Banso, *Engineering Science & Technology Journal*, **4(3)**, 84 (2023), https://doi.org/10.51594/estj.v4i3.553
3. Payal and P. Pandey, *Recent Patent Nanotechnology*, **16(1)**, 45(2022), https://doi.org/10.30574/wjarr.2024.24.1.3116
4. A.A. Beni and H. Jabbari, *Results in Engineering*, **15**, 100467(2022), https://doi.org/10.1016/j.rineng.2022.100467
5. P. Simpa, N.O. Solomon, O.A. Adenekan and S.C. Obasi, *Engineering Science & Technology Journal*, ***5*(5)**, 1710 (2024), https://doi.org/10.51594/estj.v5i5.1137

6. U.O. Aigbe and A.O. Osibote, *Journal of Hazardous Materials Advances*, **13**,100401(2024), https://doi.org/10.1016/j.hazadv.2024.100401
7. I. Levchenko, O. Baranov, C. Riccardi, H.E. Roman, U. Cvelbar, E.P. Ivanova, M. Mohandas, P. Scajev, T. Malinauskas, S. Xu and K. Bazaka, *Advanced Materials Interfaces*, **10(1)**, 2201739(2023), https://doi.org/10.1002/admi.202201739
8. N.H. Anh, M.Q. Doan, N.X. Dinh, T.Q. Huy, D.Q. Tri, B. H. Van and A.T. Le, *RSC advances*, **12(18)**, 10950(2022), https://doi.org/10.1039/D1RA08311B
9. V. Harish, M.M. Ansari, D. Tewari, M. Gaur, A.B. Yadav, M.L.G. Betancourt, F.M. Abdel-Haleem and M. Bechelany, A. Barhoum, *Nanomaterials*, **12**, 3226(2022), https://doi.org/10.3390/nano12183226
10. H. Bahrulolum, S. Nooraei, N. Javanshir, H. Tarrahimofrad, V.S. Mirbagheri, A.J. Easton and G. Ahmadian, *Journal of Nanobiotechnology*, **19**, 26(2021), https://doi.org/10.1186/s12951-021-00834-3
11. C. Pechyen, B. Tangnorawich, S. Toommee, R. Marks and Y. Parcharoen, *Sensors International*, **5**, 3511(2024), https://doi.org/10.1016/j.sintl.2024.100287
12. S.Faisal**,** H. Jan, S. A.Shah, S. Shah, A. Khan, M. T. Akbar, M. Rizwan, F. Jan, Wajidullah, N. Akhtar, A. Khattak, S. Syed and S. Syed, *ACS Omega* ,**6(14)**, 9722(2021), https://doi.org/10.1021/acsomega.1c00310
13. M.A.Dheyab, N. Oladzadabbasabadi, A.A. Aziz, P.M. Khaniabadi, M.T. Al-ouqaili, M.S. Jameel, F.S. Braim, B. Mehrdel and M. Ghasemlou, *Journal of Environmental Chemical Engineering*, **12(2)**, 112345(2024), https://doi.org/10.1016/j.jece.2024.112345
14. S. Barathi,S. Ramalingam, G. Krishnasamy and J. Lee, *Pharmaceutics*, **16(7)**, 923(2024), https://doi.org/10.3390/pharmaceutics16070923
15. A.B. Rashid, M. Haque, S.M. Islam and K.R.U. Labib, *Results in Engineering*, **22**, 102053(2024), https://doi.org/10.1016/j.rineng.2024.102053

[RJC-9211/2024]